Frequency-domain electron spin resonance spectroscopy using continuously frequency-tunable terahertz photomixers

Ohmichi, Eiji
Shoji, Yuto
Takahashi, Hideyuki
Ohta, Hitoshi

(Citation)
Applied Physics Letters,119(16):162404

(Issue Date)
2021-10-19

(Resource Type)
journal article

(Version)
Version of Record

Applied Physics Letters

Frequency-domain electron spin resonance spectroscopy using continuously frequency-tunable terahertz photomixers

Cite as: Appl. Phys. Lett. **119**, 162404 (2021); https://doi.org/10.1063/5.0065649
Submitted: 04 August 2021 • Accepted: 04 October 2021 • Published Online: 19 October 2021

Eiji Ohmichi, Yuto Shoji, Hideyuki Takahashi, et al.

Applied Physics Letters ARTICLE scitation.org/journal/apl

Frequency-domain electron spin resonance spectroscopy using continuously frequency-tunable terahertz photomixers

Cite as: Appl. Phys. Lett. **119**, 162404 (2021); doi: 10.1063/5.0065649
Submitted: 4 August 2021 · Accepted: 4 October 2021 ·
Published Online: 19 October 2021

Eiji Ohmichi,[1,a)] Yuto Shoji,[1] Hideyuki Takahashi,[1,2,3] and Hitoshi Ohta[1,2]

AFFILIATIONS

[1]Graduate School of Science, Kobe University, 1-1 Rokkodai, Nada, Kobe 657-8501, Japan
[2]Molecular Photoscience Research Center, Kobe University, 1-1 Rokkodai, Nada, Kobe 657-8501, Japan
[3]JST-PRESTO, 4-1-8 Honcho, Kawaguchi, Saitama 332-0012, Japan

[a)]Author to whom correspondence should be addressed: ohmichi@harbor.kobe-u.ac.jp

ABSTRACT

Frequency-domain electron spin resonance (FDESR) spectroscopy in the terahertz (THz) region using continuously tunable photomixers was demonstrated. Spectral resolution was greatly improved with the use of a pair of fiber stretchers. In this setup, the amplitude of the THz electric field was determined at each frequency by externally sweeping the optical path difference, resulting in a spectral resolution of about 1 MHz. With this technique, we observed narrow ESR spectra with a 20-MHz linewidth, enabling high-resolution FDESR spectroscopy in a broad frequency range.

Frequency-domain electron spin resonance (FDESR) spectroscopy[1–3] in the terahertz (THz) region has gained increasing attention, since it allows the direct determination of the energy gaps of magnetic materials. Among such materials, antiferromagnets are known to possess energy gaps called antiferromagnetic gaps. The energy scale of an antiferromagnetic gap becomes comparable to the energy of THz waves for some antiferromagnets, such as nickel oxide (NiO) and manganese oxide (MnO) [$\omega/2\pi$(NiO) $=1.1$ THz and $\omega/2\pi$(MnO) $=0.83$ THz at $T=0$ K].[4] These materials have recently attracted renewed interest for application to antiferromagnetic spintronics,[5] where antiferromagnetic magnons play essential roles in device operation. Also, zero-field splitting[6,7] is known to exist in spin systems with $S \geq 1$. The versatile functionalities of transition metal complexes and metalloproteins are often discussed in relation to the zero-field splitting. Therefore, the ability to directly access the gap is a unique advantage of FDESR over the conventional field-swept ESR technique.

The FDESR techniques reported so far have relied on either a tunable frequency source or a synchrotron radiation source. For the former, backward-traveling wave oscillators (BWOs) were often used as tunable sources.[1] However, the output power of BWO depends heavily on the frequency, so it is difficult to subtract off resonance data. Active multiplier chains,[2] combined with sweepable microwave sources, are a rapidly emerging kind of a solid-state device. Their high output powers and broad frequency ranges make them suitable for FDESR. For synchrotron radiation sources, FDESR spectra are obtained as Fourier transform of THz pulses.[3] This technique can cover the broad frequency region between 0.1 and 5 THz, where most of the interesting phenomena in low-energy magnetic excitations are observed. However, the spectral resolution of ~300 MHz is worse than that of tunable-source-based techniques.

In this study, we focused on photoconductive antenna (PCA)-based photomixers[8] as frequency-tunable sources. Photomixing of two-color cw lasers induces amplitude modulation of the photocurrent through the electrode gap of the emitter PCA, and this beat signal, whose frequency is in the THz range, generates continuous THz waves. PCA photomixers have recently emerged as unique THz sources,[8] since they allow both continuously tunable operation and high frequency resolution. Indeed, Roggenbuck *et al.*[9] reported versatile applications of the cw photomixing technique to the spectroscopy of solid-state samples. PCA photomixers have also been applied to cw electron paramagnetic resonance (EPR) spectroscopy in the THz region.[10]

Figure 1 shows a schematic diagram of the experimental setup. A commercial frequency-domain THz generation/detection system (Terascan1550, TOPTICA Photonics)[11] was employed in this study. Two distributed-feedback (DFB) lasers operating at around 1550 nm

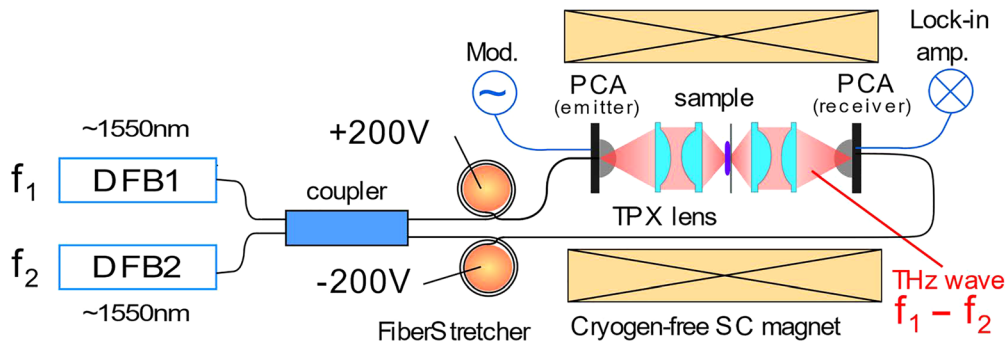

FIG. 1. Experimental setup for FDESR spectroscopy using continuously tunable PCA photomixers. All THz components, including photomixers, lenses, and a sample holder, were accommodated in a room-temperature magnet bore. Reproduced and modified with permission from Ohmichi *et al.*, Appl. Phys. Lett. **116**, 051101 (2020). Copyright 2020 AIP Publishing LLC.

were used for the generation/detection of THz waves by photomixing.[12] When two-color laser light (f_1 and f_2) is irradiated onto the gap of the emitter PCA, the current flowing in the gap is amplitude-modulated at a beat frequency $f_{\mathrm{THz}} = f_1 - f_2$, and THz waves are emitted from the bow-tie antenna. On the other hand, THz waves were detected at the receiver PCA by homodyne detection. It is noted that the emitted THz waves were linearly polarized, so that the antenna directions of both photomixers should be aligned. By changing the relative frequencies of the two lasers, a continuous tuning range of 0.05–1.1 THz was achieved. The frequency accuracy was better than 10 MHz, which was determined mainly by the stability of the DFB lasers. The typical output power was on the order of several tens of μW at 0.05 THz, but decreased rapidly to less than 1 μW at 0.5 THz.

THz waves were collimated and focused with two plano–convex lenses made of polymethylpentene (TPX).[13] A pellet-shaped sample was mounted on a polyethylene sheet and placed at the focal point of the THz waves. The beam waist at 0.3 THz was typically 0.8 mm in this setup. All optical components were assembled into a compact optical cage and inserted into the center of a cryogen-free superconducting magnet. The room-temperature sample bore of the magnet was 100 mm in diameter. It is noted that a magnetic field does not significantly affect PCA photomixers.[10] This contrasts with a situation where conventional light sources and detectors have to be placed away from the magnet center to avoid possible influences of the stray magnetic field. All measurements were carried out at room temperature. The use of PCA devices at cryogenic temperatures has been reported by Crooker,[14] but is generally difficult because the optical alignment between the laser and the PCA gap would be degraded due to thermal contraction upon cooling. Moreover, condensed water droplet may give severe electrical damages to PCA during sample exchange from a cryostat. Another way of low-temperature measurement is to use an optical cryostat equipped with optical windows, which is put in between the emitter and receiver photomixers located at room temperature.

The detected photocurrent is given by $I_{\mathrm{ph}} \propto E_{\mathrm{THz}} \cos(2\pi\Delta L f_{\mathrm{THz}}/c)$, where E_{THz} is the amplitude of the THz electric field, ΔL is the difference in the optical path length, and c is the speed of light. ΔL is given by $\Delta L = L_{\mathrm{emitter}} + L_{\mathrm{THz}} - L_{\mathrm{receiver}}$, where L_{emitter} and L_{receiver} are the optical path length from the laser to the emitter and receiver, respectively, and L_{THz} is the length between the emitter and receiver, including the sample thickness. Therefore, the photocurrent periodically oscillates due to interference when f_{THz} is swept. This indicates that in frequency-domain spectroscopy, E_{THz} has to be determined from the inherently oscillating photocurrent.

For this purpose, envelope detection is often used in the data analysis.[9] In this analysis, the amplitude and phase of the photocurrent are determined by a set of extrema of the oscillating data. Accordingly, the spectral resolution is limited by the oscillation frequency. To improve the spectral resolution, ΔL should be kept large so as to minimize the spacing between extrema, but the increment of ΔL causes intolerable drifts of the photocurrent due to the uncompensated thermal contraction of the optical fibers. Therefore, the spectral resolution is at most several hundreds of MHz in this case. Another approach was based upon Hilbert analysis, where the instantaneous E_{THz} was determined by the Hilbert transformation. With this technique, a spectral resolution of better than 10 MHz was achieved.[15,16]

In this study, we employed a different approach using a pair of fiber stretchers (PZ2-PM3-APC-E-155P, Optiphase) to precisely determine E_{THz}.[17] A fiber stretcher consists of an optical fiber cable wound around a piezo device. The fiber length can be changed by voltage application to the piezo device. Therefore, the path length ΔL can be changed to $\Delta L + \alpha V$ by externally applying the voltage V, and E_{THz} can be determined at each frequency from the oscillation amplitude of the photocurrent when the voltage ($\propto$ phase) is swept, as shown in Fig. 2(a). In this study, to maximize the phase difference, the voltage polarity for the respective fiber stretchers was set to opposite. The voltage-to-length conversion coefficient was $\alpha = 8.1\ \mu$m/V, so the maximum applied voltage of ± 200 V will produce an expected path difference of about 3.2 mm. It should be noted that two fiber stretchers must be used in order to compensate for the thermally induced phase difference of wound optical fibers.

Figure 2(a) shows the oscillating photocurrent when sinusoidal voltages with opposite polarity were applied to the respective fiber stretchers. The amplitude of oscillating current can be easily obtained if the induced phase is greater than 2π. In the case of Fig. 2(a), the total phase difference corresponded to $3.5 \times 2\pi$, and the amplitude was $|I_{\mathrm{ph}}| = 101.2$ nA. The induced phase linearly decreased with decreasing frequency, as expected, and equaled to 2π at 86.2 GHz, as shown in Fig. 2(b). Figure 2(c) shows the oscillating photocurrent and its amplitude derived from the envelope detection and the present

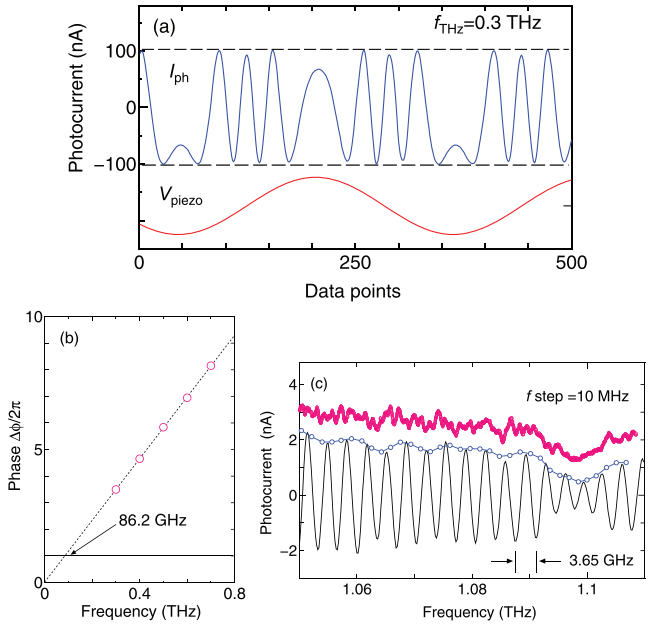

FIG. 2. (a) Photocurrent (I_{ph}) vs sampling data points, together with sinusoidal voltages (V_{piezo}) applied to the fiber stretchers. The dashed lines indicate the amplitude of the oscillating current. (b) Maximum phase induced by the fiber stretchers vs THz frequency. The dotted line indicates a linear fit to the data. (c). Oscillating photocurrent (black) vs THz frequency. The amplitude was obtained by envelope detection (blue) and the present technique (red). The data are vertically shifted for clarity.

technique. These techniques gave consistent results. The fine structures observed from the present technique were reproducible and presumably originated from multi-reflections effects of the coherent THz wave.

In cw THz spectroscopy, these oscillatory behaviors of the amplitude have been commonly observed, in particular, in the low frequency region below 0.5 THz.[18,19] When the wave lengths become comparable to the size of optical systems, the propagation of THz waves is strongly affected by reflections and diffractions, giving rise to additional spurious optical interferences. It is pointed[20] that a hemispherical silicon lens attached to PCA caused a multi-reflections inside due to a large mismatch of the refractive indexes at the interface. Indeed, the oscillatory amplitude observed in the frequency region up to 1.5 THz was analyzed in this context.[21] In the conventional setup, off-axis parabolic mirrors are usually used to minimize unfavorable multi-reflections, but in our setup, plastic lenses were inevitably used to collimate and focus THz waves due to the limited sample space. This may cause additional sources of multi-reflections at the air–plastic interfaces.

In our setup, we eventually attained a spectral resolution of 1 MHz, which was limited by frequency setting of the software at this moment. The linewidth of the DFB lasers used in our system was 650 kHz on a timescale of 100 μs.[18] This value corresponds to a beat signal linewidth of $\sqrt{2} \times 650\,\text{kHz} = 920\,\text{kHz}$. Thus, a slightly better resolution than 1 MHz might be possible without the software restriction.

In this study, a powder sample of 2,2-diphenyl-1-picrylhydrazyl (DPPH) was measured at room temperature. DPPH is known as an ESR standard sample and exhibits a temperature-independent g value ($g = 2.0036$).[22] The resonance condition of ESR absorption is theoretically given by $h\nu = g\mu_B B$,[23] where h is the Planck constant, ν is the frequency, g is the g value, μ_B is the Bohr magneton, and B is the magnetic flux density. In the high-frequency region, the linewidth of DPPH exhibits a gradual broadening[24] and the full width at half maximum (FWHM) is typically in the range of $\Delta B = 1$–2 mT in the field-sweep setup. It was reported that the linewidth depended substantially on the sample batch and the solvent from which DPPH was crystallized.[25] The frequency resolution ($\Delta\nu$) necessary for ESR detection should be better than $(\Delta B/B)\nu \sim 30$–70 MHz.

In all measurements shown below, the wave vector of THz waves was parallel to the magnetic field ($\boldsymbol{k}||\boldsymbol{B}||z$, Faraday configuration). In this setup, where oscillating magnetic field components are always orthogonal to the static magnetic field ($\boldsymbol{B}_{osc}\perp\boldsymbol{B}$), conventional ESR transitions satisfying $\Delta S_z = \pm 1$ will be observed. If the wave vector is perpendicular to the field direction ($\boldsymbol{k}\perp\boldsymbol{B}$, Voigt configuration), there are two cases: Oscillating magnetic field components $\boldsymbol{B}_{osc}$ are either perpendicular ($\perp$) or parallel ($||$) to the magnetic field $\boldsymbol{B}$. In the former case, ESR transitions similar to those in the Faraday configuration are allowed, while in the latter case, forbidden transitions ($e.g. \Delta S_z = \pm 2$) are observed for integer spin systems.[23]

Figure 3(a) shows the observed FDESR spectrum for DPPH at 3.20 T. The size of a pellet-shaped powder sample was 10 mm in diameter and 0.5 mm in thickness. The data were shown after subtraction of the background data measured at the off resonance field. Frequency was swept between 92.15 and 92.35 GHz with a step of 2 MHz. A sharp decrease in the photocurrent at 92.25 GHz was observed. In this case, the observed FWHM was $\Delta f = 20$ MHz, corresponding to $\Delta f/f \sim 2 \times 10^{-4}$. This value was much sharper than those of the typical THz absorption spectra. Indeed, the linewidth of water vapor absorption at 1.10 THz was about 9 GHz, two orders of magnitude greater than that of DPPH. We carried out similar measurements at several magnetic field values, as shown in Fig. 3(b), and confirmed that the resonance frequency shifted linearly with the applied magnetic field. In our setup, the maximum field range was limited merely by the maximum field of the magnet. Therefore, in principle, there are no experimental constraints in the frequency or in the magnetic-field range.

Figure 4 shows FDESR spectra of a mixed powder sample of DPPH and 1-oxyl-2,2,6,6-tetramethyl-4-hydroxypiperidine (TEMPOL)[26] at

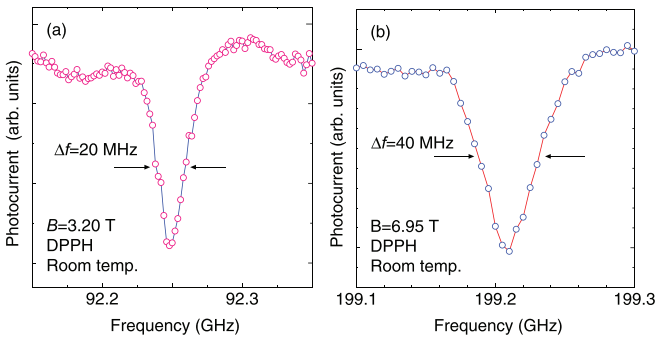

FIG. 3. FDESR spectra for DPPH radical at room temperature at (a) 3.20 and (b) 6.95 T. The frequency steps were 2 and 5 MHz, respectively.

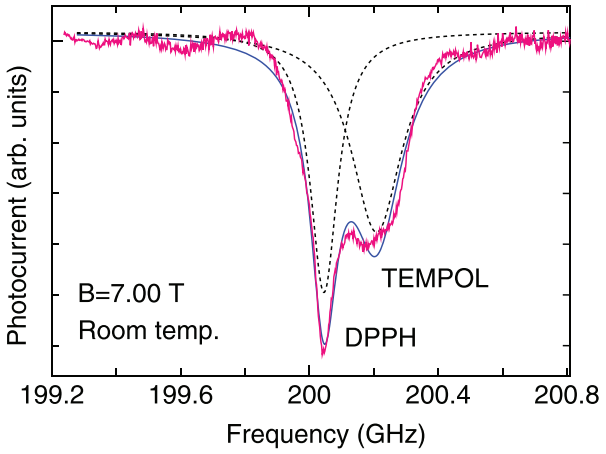

FIG. 4. FDESR spectra of a mixed powder sample of DPPH and TEMPOL at room temperature. The data (red) and a fitting curve (a solid line) composed of two Lorentzian curves (dotted lines) are shown. The frequency step was 2 MHz.

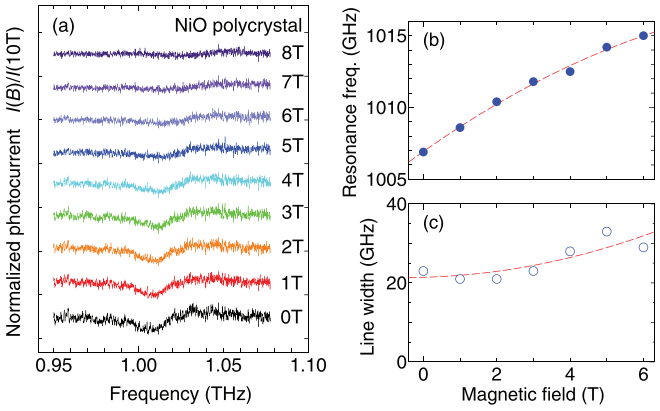

FIG. 5. (a) Normalized photocurrent $I(B)/I(10\mathrm{T})$ vs THz frequency of NiO polycrystal at various magnetic fields. The data are vertically shifted for clarity. Magnetic field dependence of (b) the resonance frequency and (c) the linewidth. The dotted lines (red) are a guide for the eyes.

7.0 T. This magnetic field value was chosen to demonstrate a benefit of high-field measurements, while keeping a substantial signal-to-noise ratio and background stability. The measurement was carried out with a frequency step of 2 MHz. The data are basically reconstructed with the sum of two Lorentzian curves. A deviation from the fitting was attributed to a long-term drift of the photocurrent induced by temperature fluctuations, arising from the optical path difference between the emitter and receiver branches. The resonance frequencies were $f_{\mathrm{DPPH}} = 200.045$ GHz and $f_{\mathrm{TEMPOL}} = 200.172$ GHz, which are consistent with $g_{\mathrm{DPPH}} = 2.0036$ and $g_{\mathrm{TEMPOL}} = 2.0062$, respectively. The two absorption lines separated by $\Delta f_{\mathrm{res}} = 127$ MHz were well resolved. The observed line widths for DPPH and TEMPOL were 103 and 192 MHz, respectively. The broader linewidth of DPPH, compared to that in Fig. 3, was due mostly to field inhomogeneity induced by sample thickness. It is known that the ESR spectrum of a TEMPOL solution sample exhibits a hyperfine structure, which is smeared out to yield a broader ESR line in solid-state samples.[27]

Finally, we show an example of the direct determination of the antiferromagnetic gap of nickel oxide (NiO) in magnetic fields. NiO is known as a collinear antiferromagnet with a Neel temperature of $T_{\mathrm{N}} = 525$ K in which ferromagnetically coupled NiO layers are stacked along the ⟨111⟩ direction alternately to exhibit the antiferromagnetic order. The spin excitation of NiO was studied previously by inelastic neutron scattering[28] and recently by more advanced techniques.[29,30] The magnetic structure has been basically understood by a two sublattice model,[28] but a more sophisticated model taking account of eight sublattices has been proposed to explain the observed antiferromagnetic resonance (AFMR) branches.[31,32]

The NiO sample used in this study was a pellet-shaped polycrystal sintered at 930 °C for 16 h. Figure 5(a) shows the frequency dependence of the photocurrent amplitude at various magnetic fields. As shown below, the resonance became broad as the magnetic field increased and was not discernible at $B = 10$ T. Therefore, the data are normalized by the photocurrent data at 10 T in order to remove field-independent components, such as the aforementioned spurious oscillatory components and water vapor absorptions (at 0.988 and 1.098 THz). This analysis makes quantitative evaluation of the linewidth more reliable. The measurements were carried out at every 100 MHz step. The data at $B = 0$ T showed a dip around 1.01 THz, which is in good agreement with the reported antiferromagnetic gap.[29] As the magnetic field increased, the resonance frequency shifted slightly to a higher side, while the linewidth increased, as shown in Figs. 5(b) and 5(c). Since the frequency shift was small, it was quite difficult to measure the field dependence of the gap by field-swept ESR techniques, but our FDESR technique makes such measurement possible in the frequency-field diagram.

For the case of an easy-plane type antiferromagnet, such as NiO, non-degenerate two magnon modes are theoretically predicted.[33] The observed mode at around 1 THz corresponds to the higher mode, which has been observed dominantly in most AFMR measurements.[34,35] The other mode predicted in much lower frequency region was not observed in this study. It is shown that field dependence of the magnon mode exhibits different behavior, depending on the field orientation.[36–38] Accordingly, the signal for a polycrystal sample should be averaged over entire field orientations, thus producing a broadening and an averaged shift of the resonance. While no effect was observed under 1.07 T in the previous literature,[34] the present results were in good agreement with these behaviors.

In this study, the spectral resolution was limited predominantly by the spectral resolution of DFB lasers used for photomixing. To further improve the spectral resolution, the use of tunable lasers with sharper line widths, such as external cavity diode lasers (ECDLs), would be interesting. The linewidth of ECDL is typically 100 kHz or less, so further improvement by two orders is possible. This extremely high spectral resolution will make it possible to resolve the hyperfine structures of dilute magnetic samples, from which more detailed analyses of the local environments of spin species would become possible.

In summary, we developed a frequency-domain ESR spectroscopy technique in the THz region using continuously tunable PCA photomixers. This technique covers the frequency range of 0.05–1.1 THz and a magnetic field range up to 10 T. To improve the spectral resolution, which was previously limited by the oscillating photocurrent, a pair of fiber stretchers were used to externally modulate the optical path difference. This technique enabled the precise

determination of the amplitude $|I_{ph}|$ at each frequency above 86 GHz, and a spectral resolution of 1 MHz was attained in this study. Using this technique, we observed sharp ESR spectra of organic radicals, whose line widths were as narrow as 20 MHz for DPPH. Also, the antiferromagnetic gap of NiO polycrystal showed a gradual shift to a higher-frequency region as well as a line broadening as the magnetic field was increased to 10 T. The compact setup and broad operating frequency of our technique are promising for versatile applications to magnetic materials with energy gaps, such as antiferromagnetic gaps and zero-field splittings.

See the supplementary material for more detailed data processing of NiO.

This work was supported by Competitive Funding Programs "Collaborative Research Based on Industrial Demand" from Japan Science and Technology Agency (JPMJSK1615) and by the Amada Foundation.

DATA AVAILABILITY

The data that support the findings of this study are available from the corresponding author upon reasonable request.

REFERENCES

[1]J. van Slageren, S. Vongtragool, B. Gorshunov, A. A. Mukhin, N. Karl, J. Krzystek, J. Telser, A. Müller, C. Sangregorio, D. Gatteschi, and M. Dressel, Phys. Chem. Chem. Phys. **5**, 3837 (2003).
[2]P. Neugebauer, D. Bloos, R. Marx, P. Lutz, M. Kern, D. Aguilà, J. Vaverka, O. Laguta, C. Dietrich, R. Clérac, and J. van Slageren, Phys. Chem. Chem. Phys. **20**, 15528 (2018).
[3]J. Nehrkorn, K. Holldack, R. Bittl, and A. Schnegg, J. Magn. Reson. **280**, 10 (2017).
[4]M. Tinkham, J. Appl. Phys. **33**, 1248 (1962).
[5]T. Jungwirth, X. Marti, P. Wadley, and J. Wunderlich, Nat. Nanotechnol. **11**, 231 (2016).
[6]J. Krzystek, A. Ozarowski, and J. Telser, Coordi. Chem. Rev. **250**, 2308 (2006).
[7]J. Lu, I. O. Ozel, C. A. Belvin, X. Li, G. Skorupskii, L. Sun, B. K. Ofori-Okai, M. Dinca, N. Gedik, and K. A. Nelson, Chem. Sci. **8**, 7312 (2017).
[8]S. Preu, G. H. Döhler, S. Malzer, L. J. Wang, and A. C. Gossard, J. Appl. Phys. **109**, 061301 (2011).
[9]A. Roggenbuck, H. Schmitz, A. Deninger, I. C. Mayorga, J. Hemberger, R. Güsten, and M. Grüninger, New J. Phys. **12**, 043017 (2010).
[10]E. Ohmichi, T. Fujimoto, K. Minato, and H. Ohta, Appl. Phys. Lett. **116**, 051101 (2020).
[11]See https://www.toptica.com/ for TOPTICA Photonics AG.
[12]Y.-S. Lee, *Principles of Terahertz Science and Technology* (Springer, Berlin, 2009), Chap. 4.
[13]See https://www.batop.de/ for BATOP GmbH.
[14]S. A. Crooker, Rev. Sci. Instrum. **73**, 3258 (2002).
[15]D. W. Vogt and R. Leonhardt, Opt. Express **25**, 16860 (2017).
[16]D.-Y. Kong, X.-J. Wu, B. Wang, Y. Gao, J. Dai, L. Wang, C.-J. Ruan, and J.-G. Miao, Opt. Express **26**, 17964 (2018).
[17]A. Roggenbuck, K. Thirunavukkuarasu, H. Schmitz, J. Marx, A. Deninger, I. C. Mayorga, R. Güsten, J. Hemberger, and M. Grüninger, J. Opt. Soc. Am. B **29**, 614 (2012).
[18]A. J. Deninger, A. Roggenbuck, S. Schindler, and S. Preu, J. Infrared Millimeter Terahertz Waves **36**, 269 (2015).
[19]L. Liebermeister, S. Nellen, R. Kohlhaas, S. Breuer, M. Schell, and B. Globisch, J. Infrared Millimeter Terahertz Waves **40**, 288 (2019).
[20]A. V. Boriskin, A. I. Nosich, S. V. Boriskina, T. M. Benson, P. Sewell, and A. Altintas, Microwave Opt. Tech. Lett. **43**, 515 (2004).
[21]M. Langenbach, A. Roggenbuck, I. C. Mayorga, A. Deninger, K. Thirunavukkuarasu, J. Hemberger, and M. Grüninger, J. Infrared Millimeter Terahertz Waves **35**, 918 (2014).
[22]N. D. Yordanov, Appl. Mag. Reson. **10**, 339 (1996).
[23]For a text, A. Abragam and B. Bleaney, *Electron Paramagnetic Resonance of Transition Ions* (Clarendon Press, Oxford, 1970).
[24]T. Tatsukawa, T. Maeda, H. Sasai, T. Idehara, M. Mekata, T. Saito, and T. Kanemaki, Int. J. Infrared Millimeter Waves **16**, 293 (1995).
[25]J. Krzystek, A. Sienkiewicz, L. Pardi, and L. C. Brunel, J. Mag. Reson. **125**, 207 (1997).
[26]T. Yoshioka, Bull. Chem. Soc. Jpn. **50**, 1372–1378 (1977).
[27]R. Stösser, W. Herrmann, U. Marx, and A. Brückner, J. Phys. Chem. A **115**, 2939 (2011).
[28]M. T. Hutchings and E. J. Samuelsen, Phys. Rev. B **6**, 3447 (1972).
[29]T. Kampfrath, A. Sell, G. Klatt, A. Pashkin, S. Meahrlein, T. Dekorsy, M. Wolf, M. Fiebig, A. Leitenstorfer, and R. Huber, Nat. Photonics **5**, 31 (2011).
[30]T. Satoh, S.-J. Cho, R. Iida, T. Shimura, K. Kuroda, H. Ueda, Y. Ueda, B. A. Ivanov, F. Nori, and M. Fiebig, Phys. Rev. Lett. **105**, 077402 (2010).
[31]M. Grimsditch, L. E. McNeil, and D. J. Lockwood, Phys. Rev. B **58**, 14462 (1998).
[32]J. Milano and M. Grimsditch, Phys. Rev. B **81**, 094415 (2010).
[33]F. L. A. Machado, P. R. T. Ribeiro, J. Holanda, R. L. Rodríguez-Suárez, A. Azevedo, and S. M. Rezende, Phys. Rev. B **95**, 104418 (2017).
[34]A. J. Sievers III and M. Tinkham, Phys. Rev. **129**, 1566 (1963).
[35]Z. Wang, S. Kovalev, N. Awari, M. Chen, S. Germanskiy, B. Green, J.-C. Deinert, T. Kampfrath, J. Milano, and M. Gensch, Appl. Phys. Lett. **112**, 252404 (2018).
[36]J. Ubbink, Physics **19**, 919 (1953).
[37]T. Nagamiya, Prog. Theor. Phys. **11**, 309 (1954).
[38]H. J. Gerritsen, Physics **21**, 639 (1955).